CrossMark

Accurate Orbital Solution for the New and Metal-poor Eclipsing Binary Tycho 5227-1023-1

G. Traven[1], U. Munari[2], S. Dallaporta[3], and T. Zwitter[1]

[1] Faculty of Mathematics and Physics, University of Ljubljana, Jadranska 19, 1000 Ljubljana, Slovenia; gregor.traven@fmf.uni-lj.si
[2] INAF Osservatorio Astronomico di Padova, I-36012, Asiago, VI, Italy
[3] ANS Collaboration, c/o Astronomical Observatory, I-36012, Asiago (VI), Italy

Abstract

The orbit and physical parameters of the previously unsolved double-lined eclipsing binary Tyc 5227-1023-1, discovered during the search for RR Lyr variable candidate members of the Aquarius stream, are derived using high-resolution échelle spectroscopy and V, i' photometry. A synthetic spectral analysis of both components has been performed, yielding metallicity $[M/H] = -0.63 \pm 0.11$ for both stars and a temperature for the secondary that is in close agreement with the one from the orbital solution, while the temperature of the primary is determined from photometry ($T_1 = 6350$ K). The masses and radii ($M_1 = 0.96 \pm 0.02$, $M_2 = 0.84 \pm 0.01\ M_\odot$, $R_1 = 1.39 \pm 0.01$, $R_2 = 0.98 \pm 0.01\ R_\odot$) reveal that both stars have already slightly evolved away from the main-sequence band, having an age of about 7 Gyr, and the results of the synthetic spectral analysis support the claim of corotation with the orbital motion. The radial velocity of the system is -60 ± 2 km s^{-1}, while its distance, computed from orbital parameters and the derived reddening $E_{B-V} = 0.053$, is 496 ± 35 pc. Even though Tyc 5227-1023-1 was initially treated as a possible member of the Aquarius stream, the results presented here disagree with reported values for this ancient structure and suggest a likely membership of the thick disk.

Key words: binaries: eclipsing – binaries: spectroscopic – Galaxy: disk – stars: fundamental parameters – stars: individual (Tycho 5227-1023-1)

Supporting material: machine-readable tables

1. Introduction

Stars are the main baryonic building blocks of galaxies, and since multiplicity is known to be common in the general stellar population (Duquennoy & Mayor 1991; Abt & Willmarth 1999; Sommariva et al. 2009; Raghavan et al. 2010; Postnov & Yungelson 2014), the wealth of information provided by multiple and especially binary systems contributes heavily to our understanding of galactic structure and evolution. Multiple systems not only play a key astrophysical role over the whole Hertzsprung–Russell (HR) diagram, but also facilitate determination of all important physical parameters, such as masses, radii, temperatures, luminosities, and distance (Torres et al. 2010; Brogaard et al. 2011, 2012).

The unique geometrical properties of double-lined eclipsing binaries (SB2 EBs) make them forerunners in the quest to obtain accurate fundamental properties of stars, first of all masses and radii, using a minimum of theoretical assumptions and modeling (Munari et al. 2004; Torres et al. 2010). Given that the component stars have the same age and initial chemical composition, eclipsing binaries represent a formidable benchmark for the validation of the current generation of stellar evolutionary models (Andersen 1991; Lastennet & Valls-Gabaud 2002 and references therein).

The photometric variability of eclipsing binary Tyc 5227-1023-1 (R.A.: 22 00 52.6 decl.: −03 42 12.4, J2000) was first noted by Munari et al. (2014c), who reported about 180 new field variables discovered as a by-product of the search for RR Lyr variable candidate members of the Aquarius stream (Munari et al. 2014a).

The RAVE Survey enabled the discovery of the Aquarius stream by Williams et al. (2011), describing a chemically coherent structure that originates from the tidal disruption of a 12-Gyr-old [α/Fe]-enhanced globular cluster of low metallicity ([Fe/H] = −1.0; Wylie-de Boer et al. 2012). The stream appears to be on a trajectory toward the solar neighborhood from the direction of Aquarius. The velocity of the infalling stream members increases as they reach the disk of the Galaxy, from −160 to −210 km s^{-1}, with smaller velocities pertaining to the most distant known members at about 3 kpc, and larger ones for those closer to us at about 1 kpc. However, fitting the stellar parameters of stream members to isochrones produces only a crude estimate for their distance. It is therefore important to identify more members and derive robust distances to them, thus enabling the reconstruction of the stream's Galactic orbit and three-dimensional shape, along with constraining the Galactic gravitational potential in the solar vicinity.

The scarce epoch photometry available to Munari et al. (2014c) did not allow us to classify the type of variability exhibited by Tyc 5227-1023-1. We initially acquired some additional photometric data that suggested it to be an eclipsing binary, and an exploratory high-resolution optical spectrum proved it to be a double-lined binary of low metallicity. This immediately boosted our interest in the object, and a full-scale observing campaign was initiated that aimed to obtain an accurate orbital solution and therefore a geometrical distance to Tyc 5227-1023-1. Accurate orbital solutions for high Galactic latitude, metal-poor binaries are rare, and this alone could justify the present investigation. Should our target turn out to be a member of the Aquarius stream, this would further boost the interest in it.

2. Observational Data

2.1. Photometry

CCD photometry in the Landolt V and SLOAN i' bands of Tyc 5227-1023-1 has been obtained with ANS Collaboration

Table 1
CCD Photometry in the Landolt V and SLOAN i' Bands of Tyc 5227-1023-1

HJD	Phase	V	err	i'	err
841.560	−0.5657	11.920	0.012	11.655	0.009
842.532	−0.3400	11.924	0.006	11.649	0.005
842.574	−0.3302	11.924	0.003	11.643	0.005
850.545	−0.4792	11.974	0.008	11.693	0.007
857.489	−0.8665	11.933	0.004	11.660	0.004

Note. The columns give the heliocentric JD (-2456000), the orbital phase, and the magnitudes with their uncertainties.

(This table is available in its entirety in machine-readable form.)

telescope N. 36, which is a 0.30 m Ritchey–Cretien telescope located in Cembra (Trento, Italy). It is equipped with an SBIG ST-8 CCD camera, 1530×1020 array, 9 μm pixels $\equiv$ $0\rlap.{''}77$/pix, with a field of view of $19' \times 13'$. The V and i' filters are from Schuler and Astrodon, respectively. The data are given in Table 1 (available in full only electronically), where the quoted uncertainties are the total error budget, combining quadratically the measurement error on the variable with the error of the transformation from the instantaneous local photometric system to the standard one, as defined by the local photometric sequence extracted from the APASS survey (Henden et al. 2012; Munari et al. 2014c), which is calibrated against the Landolt (2009) and Smith et al. (2002) equatorial standards. Technical details of the ANS Collaboration network of telescopes running since 2005, their operational procedures, and sample results are presented by Munari et al. (2012). A detailed analysis of the photometric performances and measurements of the actual transmission profiles for all of the photometric filter sets in use is presented by Munari & Moretti (2012). All measurements on Tyc 5227-1023-1 were carried out with aperture photometry, the long focal length of the telescope, and the absence of nearby contaminating stars not requiring the use of point-spread function (PSF) fitting.

2.2. Spectroscopy

Spectra of Tyc 5227-1023-1 were secured in 2015–2016 with the échelle+CCD spectrograph mounted on the 1.82 m telescope operated by Osservatorio Astronomico di Padova atop Mt. Ekar (Asiago). The instrumentation and observing setup match those described by Siviero et al. (2004), to which we refer for details of the observing mode. Here we recall that the 3600–7400 Å wavelength region is covered in 30 orders at a resolving power of 20,000. A journal of the observations is given in Table 2 for 26 obtained spectra with exposure times of 1200, 1800, and one of 2700 s, which provide a moderate signal-to-noise ratio (S/N) while avoiding smearing due to the orbital motion (1500 s corresponds to less than 2% in orbital period). The first spectrum listed in the table was recorded practically at zero phase (hereafter the PH_0 spectrum) and was used to measure the systemic velocity and as a template for radial velocity (RV) measurements.

The spectra have been extracted and calibrated in a standard fashion with IRAF. The wavelength solution has been derived simultaneously for all 30 recorded échelle orders, with an average rms of 0.32 km s^{-1}.

2.3. Systemic Velocity

The systemic velocity of Tyc 5227-1023-1 is measured on the PH_0 spectrum. The fxcor routine in IRAF is applied to 22 échelle orders #34–55 [4000–6700 Å], using a similar synthetic spectrum selected from the Munari et al. (2005) synthetic spectral atlas computed at the same 20,000 resolving power as the échelle scientific spectra. The average value of the systemic radial velocity is -62.47 km s^{-1} with the uncertainty of 2 km s^{-1} (see Table 3). This value is later adjusted by the orbital solution (see Section 3.4).

2.4. Radial Velocities

We use TODCOR, a two-dimensional cross-correlation algorithm (Zucker & Mazeh 1994), to derive the radial velocities. This technique obtains Doppler shifts of both stellar components simultaneously by employing a multiple-correlation approach, producing at the same time their intensity ratio. We apply it to the 22 échelle orders #34–55 covering the 4000–6700 Å range. Each order is trimmed 25% at both ends, corresponding to a redundant region where adjacent orders overlap. The lower instrument response in these end regions leads to (1) degradation of the wavelength solution accuracy, (2) poorer S/N, and (3) a steeper continuum since normalization to unity is more difficult. Retaining only the central 50% of each order alleviates these issues.

The PH_0 spectrum was used as the template for TODCOR in deriving radial velocities. The reason for using a larger number of orders than what is detailed in Siviero et al. (2004) is the lower S/N of spectra in this study, resulting in some of the solutions from arbitrary orders being invalid (e.g., both radial velocities being either larger or smaller than the systemic velocity). The radial velocity values from individual orders are also rejected if they lie outside the 2.5σ of their distribution, which removes the remaining anomalies. On average, results from 12 orders out of 22 are kept, and the final values of radial velocities are summarized in Table 2. The mean uncertainty of values used in the orbital solution (see Section 3) is 3.32 km s^{-1} for star 2 (the fainter of the two) and 1.81 km s^{-1} for star 1. The small variations in the temperature of the template do not have a significant effect on the TODCOR results.

3. Orbital Solution

A simultaneous spectroscopic and photometric solution for Tyc 5227-1023-1 was obtained with the PHOEBE 0.31 code (Prša & Zwitter 2005a, 2005b), which is based on the models of Wilson & Devinney (1971) and Wilson (1979). Orbital modeling was performed using the *detached binary* system option in PHOEBE, appropriate for our case. The solution of the binary system is obtained following the Bayesian approach to parameter estimation, employing a Markov chain Monte Carlo (MCMC) Ensemble sampler *emcee* (Foreman-Mackey et al. 2013). At each step in the surveyed parameter space, a PHOEBE orbital solution is computed, with the initial starting point randomly determined from uniform priors. The effective temperature of star 1 and the metallicity for both stars are determined and fixed in an iterative procedure of combining results from (1) the orbital solution, (2) available photometric data, and (3) atmospheric analysis (see Sections 3.1, 3.2, and Table 3), while the remaining parameters of the binary system are adjusted. A logarithmic law for limb darkening is assumed

Table 2
Heliocentric Radial Velocities (km s^{-1}) of Tyc 5227-1023-1

#	HJD	Phase	t	Star 1		Star 2		$\langle S/N \rangle$
				RV	err	RV	err	
56808	326.289	0.9999	1800					23
56836	327.282	0.2305	1800	−73.0	1.6	85.7	2.0	31
56891	328.284	0.4631	1800	−14.9	1.9	14.9	4.8	28
56953	329.326	0.7052	1800	71.7	1.0	−80.7	1.0	31
56986	330.232	0.9155	1800	39.5	1.6	−39.9	2.1	32
57011	350.280	0.5711	1800	36.3	4.1	−31.4	6.1	22
57277	380.225	0.5251	1200	16.2	2.0	−5.5	2.1	20
58030	586.577	0.4450	1800	−23.5	1.8	32.2	5.1	22
58053	587.555	0.6721	1200	65.2	2.3	−73.3	2.1	16
58055	587.572	0.6760	1200	68.1	1.5	−75.5	3.0	17
58057	587.589	0.6799	1200	67.2	1.4	−78.3	3.5	18
58074	588.550	0.9032	2700	45.7	1.3	−44.6	2.5	31
58592	736.222	0.1959	1800	−69.3	1.5	81.5	1.9	18
58593	736.244	0.2011	1800	−67.8	2.0	84.5	3.8	23
58594	736.266	0.2062	1800	−69.3	1.5	83.6	2.8	24
58666	738.234	0.6633	1800	67.3	1.9	−69.7	2.8	26
58667	738.257	0.6687	1800	68.6	1.1	−68.2	1.7	26
58710	739.205	0.8889	1800	50.4	2.5	−49.6	2.5	24
58712	739.231	0.8948	1800	48.4	1.5	−49.9	2.1	26
58799	741.231	0.3592	1800	−55.2	1.9	63.9	11.1	19
57068	351.312	0.8107	1800	74.6	1.6	−74.9	1.8	18
57337	384.221	0.4530	1800	−25.4	2.1	21.7	3.4	25
58120	590.574	0.3732	3600	−38.7	2.6	61.2	2.6	24
58753	740.218	0.1239	1800	−46.2	1.8	53.8	1.8	23
58755	740.242	0.1295	1800	−50.7	1.5	49.3	1.5	25
58757	740.265	0.1349	1800	−52.1	1.5	55.6	8.5	22

Notes. The columns give the spectrum number (from the Asiago échelle log book), the heliocentric JD (−2457000), the orbital phase, the exposure time (s), the radial velocities of the two components in km s^{-1}, and the corresponding uncertainties. The last column gives the S/N of the spectrum (per pixel) averaged over the wavelength range considered in the radial velocity analysis. Listed in the last six rows are RV values that are rejected from the solution (see Section 3).

(This table is available in machine-readable form.)

using the native PHOEBE limb-darkening tables for the appropriate T_{eff}, log g, and [M/H], computed per passband. The RV measurements outside the 2.5σ of their distribution around the solution are iteratively rejected and are listed as the last six rows of Table 2 and marked in Figure 1. In row order, the first five of these are rejected after the first orbital solution converges, the last one after the second solution, and none are rejected after the third (final) solution. The solutions converged after ∼7000 MCMC iterations employing 256 walkers. For check and completeness, we rerun full orbital solutions also with linear and square-root limb-darkening laws, as well as for metallicities [M/H] = [M/H]$_{fixed}$ ± 0.2. The response of the orbital solution to these changes was minimal, with orbital parameters not varying by more than their uncertainties.

3.1. Effective Temperature of the Primary Star

An initial estimate of the spectral type of Tyc 5227-1023-1 was done by visual comparison of a low-resolution spectrum to the spectral classification standard stars and evaluated to G2 V (5860 K)–G3 V (5770 K). The temperatures are taken from Bertone et al. (2004) ATLAS results for dwarfs, and the low-resolution spectrum was obtained with the Asiago 1.22 m telescope + B&C spectrograph. However, considering the low metallicity, which could have affected the spectral classification in this part of the HR diagram, we prefer to rely on the $B - V$ color index, for which high-quality direct T_{eff} calibrations exist, while they are missing for $V - i'$.

We obtain the T_{eff} for star 1 with the transformation of Tycho photometry to the Johnson system following Bessell (2000). The uncertainties of the Tycho B_T and V_T are 0.32 and 0.27 (Høg et al. 2000), indicating the dispersion of the measures due to Tyc 5227-1023-1 being a variable with amplitude >0.3 mag, but this does not reflect into a wrong mean value.[4] The reddening from Section 3.3 is used to derive $(B - V)_0 = (B - V) - E_{B-V} = 0.55 - 0.053 = 0.497$. With star 1 slightly evolved from the main sequence (see Table 3 and Figure 2), this translates to $T_1 = 6350$ and the spectral type of F7IV-V, following Fitzgerald (1970) and Bertone et al. (2004). Taking into account the color–T_{eff} relation and its dependence on metallicity, reddening, and photometric system transformations, the uncertainty on T_1 is evaluated to 200 K. The excellent agreement of the derived temperatures with the position of the stars on the isochrones and evolutionary tracks in Figure 2 confirmed for us the choice of T_1.

3.2. Atmospheric Analysis

Considering the moderate S/N of our échelle spectra, it is not feasible to resolve the degeneracy among the stellar parameters by means of synthetic spectral fitting. Nevertheless,

[4] We have checked the soundness of $B_T - V_T = 0.59$ reported in the Tycho catalog by imaging the field around Tyc 5227-1023-1 (observation outside of the eclipse), including other Tycho stars for comparison, whereby deriving a value of $B_T - V_T = 0.55 \pm 0.06$, which is in good agreement with the one from the catalog.

Table 3
Orbital Solution (Overplotted to the Observed Data in Figure 1) and
Atmospheric Parameters from the χ^2 Fit to
Synthetic Spectra for Tyc 5227-1023-1

		Orbital solution	
P	(day)	4.306192	$^{+0.000004}_{-0.000004}$
T_0	(HJD)	2457003.3261	$^{+0.0002}_{-0.0002}$
K_1	(km s^{-1})	74.4	$^{+0.5}_{-0.5}$
K_2	(km s^{-1})	84.7	$^{+0.7}_{-0.7}$
a	($R_\odot$)	13.5379	$^{+0.0681}_{-0.0644}$
V_γ	(km s^{-1})	2.12	$^{+0.34}_{-0.34}$
$q = \frac{m_2}{m_1}$	(deg)	0.8777	$^{+0.0094}_{-0.0091}$
i		88.87	$^{+0.18}_{-0.13}$
e		0.00029	$^{+0.00013}_{-0.00012}$
T_1–T_2	(K)	403	$^{+7}_{-7}$
Ω_1		10.63	$^{+0.05}_{-0.04}$
Ω_2		13.23	$^{+0.16}_{-0.16}$
r_1	(R_1/a)	0.1026	$^{+0.0005}_{-0.0005}$
r_2	(R_2/a)	0.0721	$^{+0.0007}_{-0.0006}$
R_1	($R_\odot$)	1.388	$^{+0.010}_{-0.010}$
R_2	($R_\odot$)	0.977	$^{+0.011}_{-0.009}$
M_1	($M_\odot$)	0.9560	$^{+0.0167}_{-0.0155}$
M_2	($M_\odot$)	0.8391	$^{+0.0123}_{-0.0114}$
$M_{bol,1}$		3.61	$^{+0.02}_{-0.02}$
$M_{bol,2}$		4.66	$^{+0.02}_{-0.02}$
$\log g_1$	(cgs)	4.13	$^{+0.01}_{-0.01}$
$\log g_2$	(cgs)	4.38	$^{+0.01}_{-0.01}$
distance	(pc)	496	$\pm$ 35
		Photometric temperature	
T_1	(K)	6350	$\pm$ 200
		Atmospheric analysis	
T_2	(K)	5923	$\pm$ 213
[M/H]		−0.63	$\pm$ 0.11
		Systemic velocity	
V_{sys}	(km s^{-1})	−60.35	$\pm$ 3

Note. For parameters derived by PHOEBE (*orbital solution*), uncertainties from posterior distributions are reported (see Figure 3 in Appendix), whereas for others, as well as for the distance to the system, we state the most reliable and propagated uncertainty estimates. T_1 is derived from photometry and fixed in the orbital solution, which adjusts only the difference $T_1 - T_2$ (in this case the ratio of both temperatures). Propagation of the uncertainty of T_1 onto other derived properties and general remarks on results in this table are discussed in Section 4.

we use a straightforward atmospheric analysis, performing a simultaneous χ^2 fitting of both components together with the constraints from the orbital solution to derive the metallicity of both stars and to check their rotational velocities for orbital/rotational synchronization. This is done on the two most appropriate scientific exposures close to quadrature (56953 and 56836 in Table 2), using the synthetic atlas of spectra (Munari et al. 2005). For a more reliable convergence, only six adjacent échelle orders (#40–45) that cover the wavelength range 4890–5690 Å were selected for their position close to the optical axis of the spectrograph where optical quality is the best and the S/N reaches peak values. Before fitting, each order was trimmed so as to retain only the central 25%, where the

instrumental response and PSF sharpness are the best, providing a measured average resolving power of 18,000.

The temperature of star 1 is derived from photometry as described in Section 3.1, while the appropriate grid of temperatures for star 2 and metallicities, obtained with linear interpolation, was chosen ($T_{step} = 10$ K, [M/H]$_{step}$ = 0.05). The low reddening and the similarity of the two stars allow us to set the luminosity ratio ($L_2/L_1 = 0.38$) and the surface gravities as given by the orbital solution. Fixing the synchronized rotational velocities based on the orbital solution always produces a better fit. The results of atmospheric analysis therefore support the claim of rotational synchronization and provide metallicity as the fundamental parameter of the system along with the temperature of star 2.

3.3. Reddening and Distance

To derive the photometric temperature of the system and compute the distance to Tyc 5227-1023-1 from the orbital solution, reddening is evaluated by adopting the statistical 3D approach of Munari et al. (2014b), which works particularly well for the region of Aquarius. This model is essentially based on a homogeneous slab of dust extending for 140 pc on either side of the Galactic plane, causing a reddening of $E_{B-V} = 0.036$ at the poles. We obtain the first distance estimate by neglecting the reddening and using only a bolometric correction for star 1 (BC$_1 = -0.006$) and star 2 (BC$_2 = -0.052$). After confirming that our system is well beyond the region of dust in our model, a color excess $E_{B-V} = 0.053$ is determined and used in the standard $A_V = E_{B-V} \times 3.1$ reddening law. The bolometric correction is calculated in iteration with the derived temperatures of both stars, employing the prescription from Torres (2010). Using the above values, the final distance is computed together with the rest of the parameters in the orbital solution with PHOEBE.

3.4. Physical Parameters

Final values of parameters with the most reliable uncertainty estimates for the Tyc 5227-1023-1 binary system are given in Table 3. Although the systemic velocity V_{sys} is measured on the PH$_0$ spectrum, used as a template for TODCOR to derive radial velocities of other spectra, the V_γ parameter was nevertheless left free to be adjusted, due to the uncertainty in the V_{sys} determination. In the final solution, V_{sys} is corrected for the value of V_γ.

To sample the convergence and achieved minimum of the χ^2 fit in atmospheric analysis, we retain the best 50 results, yielding the temperature of star 2 (5923 $\pm$ 73 K) and metallicity (−0.63 $\pm$ 0.02). All system parameters are well constrained by the orbital solution in Table 3, with formal accuracies of 1.7 and 1.5% on the masses and 0.8 and 1.1% on the radii. The synchronized rotational velocities of the two stars would be 16.3 and 11.5 km s^{-1}. The temperature of star 2 ($T_2 = 5947$ K) is in good agreement with that from the χ^2 atmospheric fit ($\triangle T_2 = 24$ K).

The posterior distributions of parameters adjusted in the PHOEBE orbital solution with MCMC are plotted in Figure 3 in the Appendix. The values of these parameters in Table 3 and their uncertainties are determined from the 16th, 50th, and 84th percentiles of their distributions.
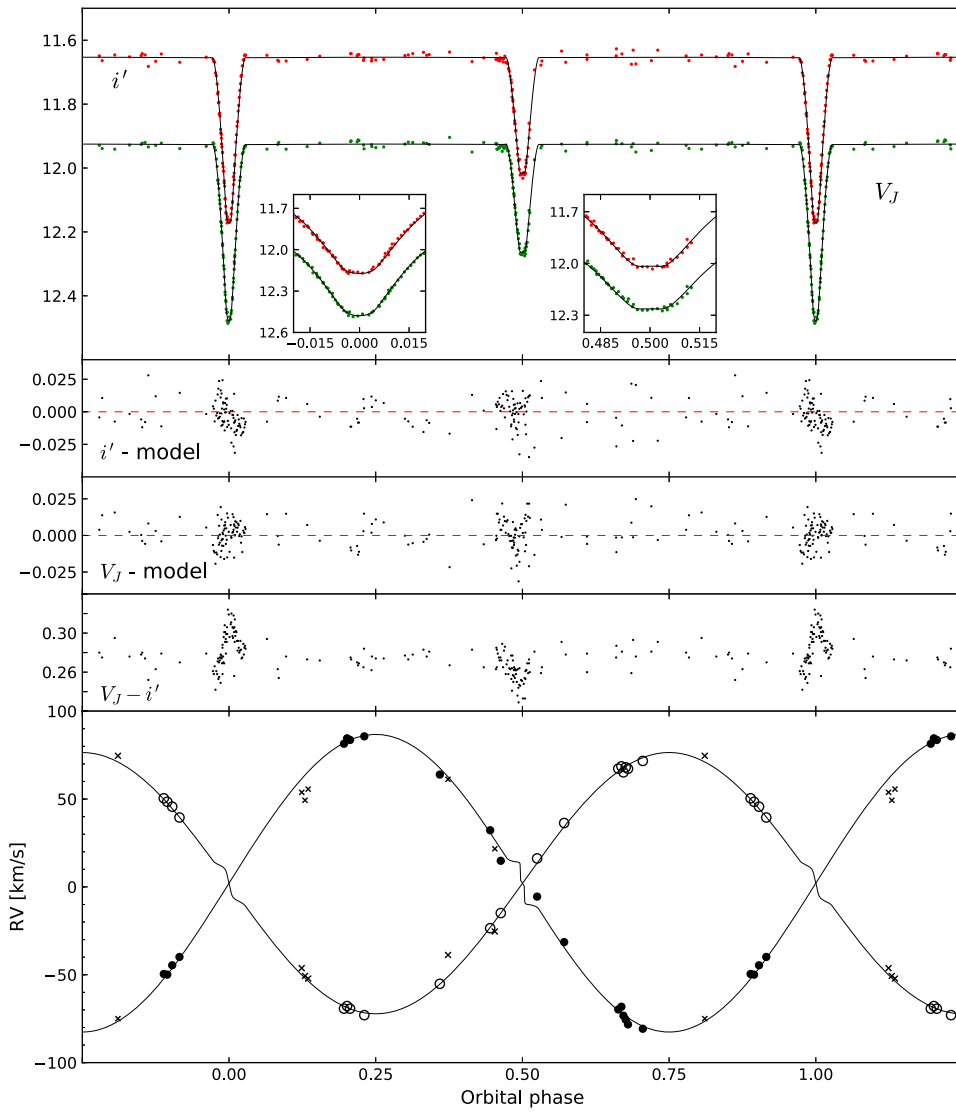
Figure 1. Our V_J, i', i'-model, V_J-model, V_J - i', and radial velocity data of Tyc 5227-1023-1. In the radial velocity panel, the open circles indicate the hotter and more massive star 1, while the solid circles pertain to the cooler and less massive star 2. The RV values for the PH$_0$ spectrum are not plotted, while RV values rejected from the solution (see Section 3) are marked by x's. The orbital solution from Table 3 is overplotted to the data and used in the second and third panels from the top.
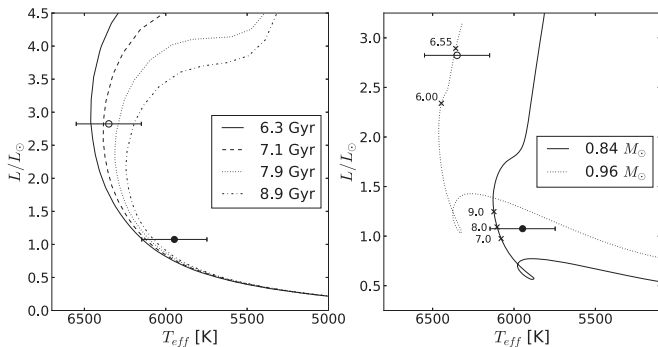
Figure 2. Comparison of both stars' temperature and luminosity as given in the orbital solution (see Table 3) with those produced by theoretical stellar models. Plots contain Padova theoretical isochrones and evolutionary tracks, which have been derived by interpolating adjacent points from the computed grid (0.8–0.85 and 0.95–1 $M_\odot$, and 0.002 and 0.004 for Z). Open circles denote the hotter and more massive star 1, whereas solid circles refer to the cooler and less massive star 2. The age on the evolutionary tracks is marked in Gyr. The error bars on star 1 indicate the uncertainty of photometric evaluation for T_1, while those on star 2 are slightly larger due to the additional uncertainty from the orbital solution for T_2.

3.5. Comparison with Theoretical Stellar Models

We compare the physical parameters from the orbital solution of Tyc 5227-1023-1 with Padova theoretical models (Bressan et al. 2012; Tang et al. 2014, and references therein). The position of the two components on the L, $T_{\rm eff}$ plane is presented in Figure 2, where a comparison is provided with isochrones and evolutionary tracks appropriate for the masses (0.96 and 0.84 $M_\odot$) and metallicity ([M/H] = log $Z/Z_\odot$ = -0.63, where $Z = 0.0035$ and $Z_\odot = 0.0152$) of the system components, while rotations of the stars are not taken into account. They have been obtained by interpolation over the grid computed by the Padova theoretical group. The agreement between theoretical models and the more reliable solution for star 1 (the primary) predicts the binary's age of about 7 Gyr.

4. Discussion

The physical parameters of Tyc 5227-1023-1 suggest that both components of the binary system have already slightly evolved from the main sequence. We are able to derive masses

and radii of both stars to formal accuracies of 2% or better. However, we note that while the formal accuracies of the orbital solution are excellent due to the very high quality photometric data and reasonably accurate radial velocities, there are other factors that have to be taken into account. The comparison of the orbital solution to photometry data in Figure 1 shows a slight asymmetry in the region of the minima, which could be explained by the inclusion of third light in the fit, the atmospheric conditions and calibration of photometric observations at different epochs, or by the actual activity of the stars. A possible third body in the system might also contribute to the time variations in the light curve. All these effects can influence the radii determination given in Table 3 and increase their uncertainty. We also investigate certain other contributions to the uncertainty on the masses from Table 3 by (1) fixing the eccentricity to zero; (2) removing all but a few photometry data points from the fit, so as to not have the solution affected or driven primarily by the light curve; and (3) removing the offset to the RV of the system (V_γ parameter) from the fit, where V_{sys} is determined from the PH_0 spectrum. In the first two cases, the uncertainty on masses determined by the MCMC procedure is almost the same, whereas the change in value of both masses is much less than their uncertainty given in Table 3. The third case, however, produces a significant effect of reducing the primary's mass by 1σ compared to the value given in Table 3.

Some of our results are furthermore affected by uncertainties in evaluating the bolometric correction, reddening, and especially the primary's (star 1) effective temperature, which was determined with color–T_{eff} relations. In this respect, the uncertainty for the distance given by the PHOEBE orbital solution (± 3 pc) has to be corrected for the fact that T_1 is evaluated with an accuracy of ± 200 K, yielding a final uncertainty on the distance to the system of ± 35 pc. The atmospheric analysis (Section 3.2) is likewise affected by the temperature uncertainty, producing higher metallicity values for increasing temperatures and lower values for decreasing temperatures. The propagated uncertainty on metallicity (± 0.11) is therefore larger than the one given in Section 3.2. Taking the uncertainty on both temperatures and metallicity into account, the position of the stars on evolutionary tracks would shift significantly, producing an uncertainty in age of ± 1 Gyr, with a younger age corresponding to lower temperatures and metallicity. However, the comparison to theoretical models becomes much less reliable when scaling these parameters by their uncertainty.

Observationally, the binary system with its visual magnitude $V = 11.86$ is relatively faint for our instrument and would necessitate much longer exposure times to reach higher values of S/N. This was not feasible for several reasons, including the position on the sky at the time of observations. The observed object was often relatively low above the horizon, reaching only $40°$ at culmination. Nevertheless, there is good agreement between the atmospheric analysis and the orbital solution by PHOEBE, where the photometrically derived spectral type and the temperature of the primary are supported by theoretical stellar models. Therefore, we are able to present a reliable solution of the system, together with the estimate of its distance at 496 pc and a conservative age of 7 Gyr, based on the primary star's position on isochrones and

evolutionary tracks, where the 1 mag fainter secondary is expectedly less well constrained.

There is an indication of alpha enhancement in our spectra, complying with the properties of the Aquarius stream and the thick disk, but it is detected only when extending the synthetic spectral analysis toward bluer wavelengths, where the results for other parameters become less reliable due to lower S/N. Nevertheless, the systemic velocity (-60 km s^{-1}), metallicity (-0.63), and age (≈ 7 Gyr) of Tyc 5227-1023-1 differ from those assigned to members of the Aquarius stream ($-240 < RV < -160$ km s^{-1}, [M/H] $= -1.0$, age ≈ 12 Gyr), so despite the possibility of a partnership to this tidally disrupted structure, which was among the initial drivers for this study, the results of the modeling and atmospheric analysis with χ^2 fit in the end disprove it.

Tyc 5227-1023-1 has consistent chemistry but relatively high velocity with regard to the thick disk (typical velocity dispersion $\sigma_z \approx 34$ km s^{-1}, Sharma et al. 2014), whereas it would kinematically comply well with the galactic halo, although being on the metal-rich end of halo stars, reminiscent of the recently discovered metal-rich halo star born in the Galactic disk (Hawkins et al. 2015). In the latter proposition, however, the dynamical ejection from the thick disk into the halo does not seem likely, due to this system's mass and binary nature.

The first official release of *Gaia* data (DR1; Gaia Collaboration et al. 2016) for stars from the Tycho catalog gives a parallax measurement of 2.11 ± 0.8 mas (473 ± 180 pc), which is in very good agreement with our result on the distance to the system (496 ± 35 pc). Using the numerical integrator NEMO (Teuben et al. 1995; Barnes et al. 2010) and the results presented in this work complemented by the *Gaia* astrometric solution (pmRA = 47.67 ± 2.98 mas yr^{-1}, pmDE = -8.1 ± 1.44 mas yr^{-1}), we derive a highly eccentric orbit ($e \approx 0.77$, $i \approx 7°$), having a pericenter and apocenter at 1.1 and 8.6 kpc, respectively. For this approximate orbit evaluation, the maximum height above the galactic plane (≈ 575 pc) is consistent with the thick disk population.

Appendix
Posterior Distributions of Adjusted Parameters

Posterior distributions are available for all adjusted parameters from Table 3 and a few more that PHOEBE uses internally. Because of their compact representation in the
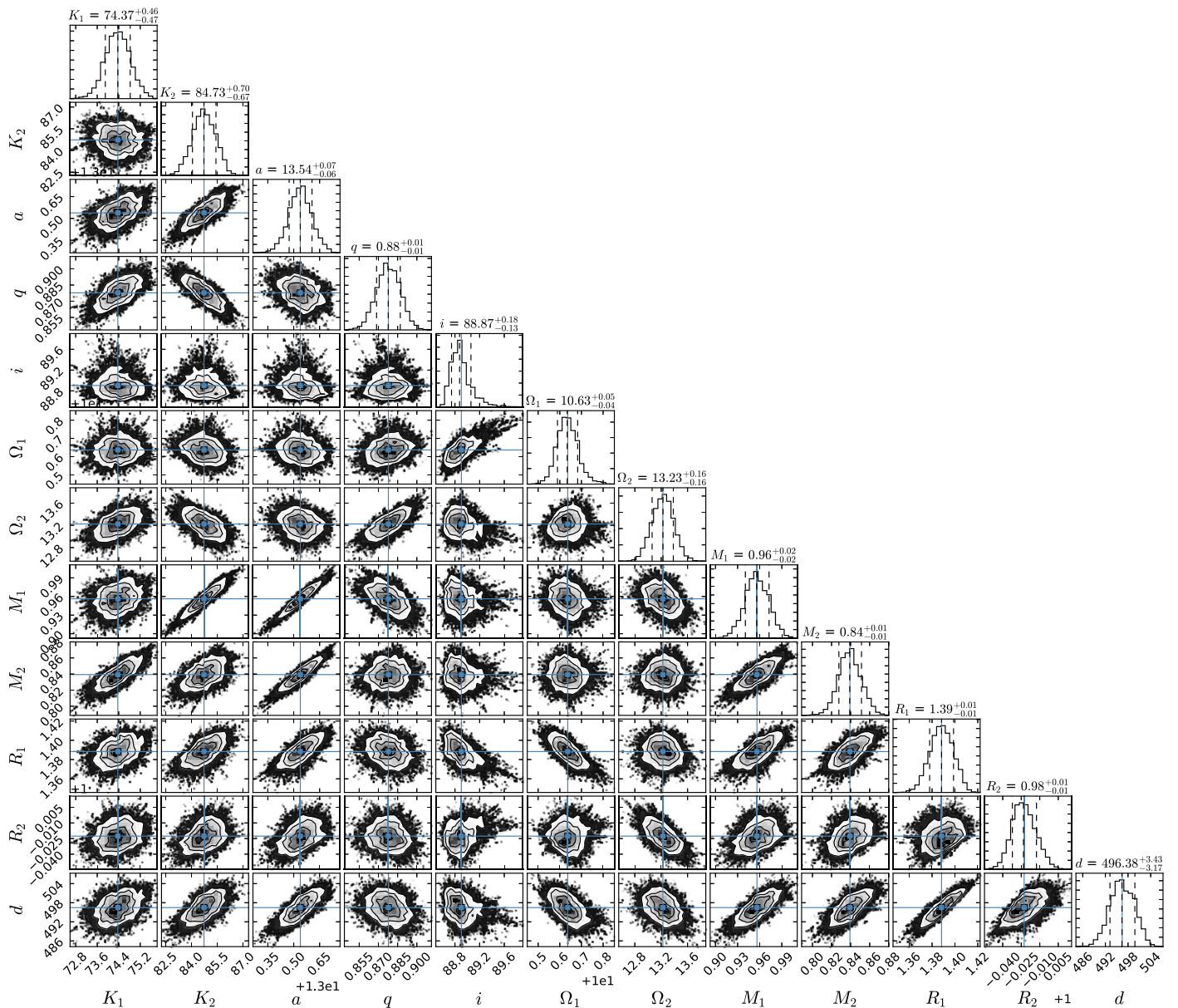
Figure 3. The parameter distributions include all values of 256 walkers for the last 1000 iterations after convergence of the orbital solution. The tiles visualize parameter posteriors (diagonal) and parameter correlations (lower left). Dashed lines in posteriors represent the 16th, 50th, and 84th percentiles, while the solid lines in all subpanels mark the mean value.

triangle plot and for easier viewing, only the most interesting ones are shown in Figure 3.

References

Abt, H. A., & Willmarth, D. W. 1999, ApJ, 521, 682
Andersen, J. 1991, A&ARv, 3, 91
Barnes, J., Hut, P., & Teuben, P. 2010, NEMO: A Stellar Dynamics Toolbox, Astrophysics Source Code Library, ascl:1010.051
Bertone, E., Buzzoni, A., Chávez, M., & Rodríguez-Merino, L. H. 2004, AJ, 128, 829
Bessell, M. S. 2000, PASP, 112, 961
Bressan, A., Marigo, P., Girardi, L., et al. 2012, MNRAS, 427, 127
Brogaard, K., Bruntt, H., Grundahl, F., et al. 2011, A&A, 525, A2
Brogaard, K., VandenBerg, D. A., Bruntt, H., et al. 2012, A&A, 543, A106
Duquennoy, A., & Mayor, M. 1991, A&A, 248, 485
Fitzgerald, M. P. 1970, A&A, 4, 234
Foreman-Mackey, D. 2016, The Journal of Open Source Software, 1 https://doi.org/10.211052Fjoss.00024

Foreman-Mackey, D., Hogg, D. W., Lang, D., & Goodman, J. 2013, PASP, 125, 306
Gaia Collaboration, Brown, A. G. A., Vallenari, A., et al. 2016, A&A, 595, 2
Hawkins, K., Kordopatis, G., Gilmore, G., et al. 2015, MNRAS, 447, 2046
Henden, A. A., Levine, S. E., Terrell, D., Smith, T. C., & Welch, D. 2012, JAVSO, 40, 430
Høg, E., Fabricius, C., Makarov, V. V., et al. 2000, A&A, 355, L27
Landolt, A. U. 2009, AJ, 137, 4186
Lastennet, E., & Valls-Gabaud, D. 2002, A&A, 396, 551
Munari, U., Bacci, S., Baldinelli, L., et al. 2012, BaltA, 21, 13
Munari, U., Dallaporta, S., Siviero, A., et al. 2004, A&A, 418, L31
Munari, U., Henden, A., & Frigo, A. 2014a, NewA, 27, 1
Munari, U., Henden, A., Frigo, A., et al. 2014b, AJ, 148, 81
Munari, U., Henden, A., Frigo, A., & Dallaporta, S. 2014c, JAD, 20, 4
Munari, U., & Moretti, S. 2012, BaltA, 21, 22
Munari, U., Sordo, R., Castelli, F., & Zwitter, T. 2005, A&A, 442, 1127
Postnov, K. A., & Yungelson, L. R. 2014, LRR, 17, 3
Prša, A., & Zwitter, T. 2005a, ApJ, 628, 426
Prša, A., & Zwitter, T. 2005b, Ap&SS, 296, 315
Raghavan, D., McAlister, H. A., Henry, T. J., et al. 2010, ApJS, 190, 1
Sharma, S., Bland-Hawthorn, J., Binney, J., et al. 2014, ApJ, 793, 51

Siviero, A., Munari, U., Sordo, R., et al. 2004, A&A, 417, 1083
Smith, J. A., Tucker, D. L., Kent, S., et al. 2002, AJ, 123, 2121
Sommariva, V., Piotto, G., Rejkuba, M., et al. 2009, A&A, 493, 947
Tang, J., Bressan, A., Rosenfield, P., et al. 2014, MNRAS, 445, 4287
Teuben, P. 1995, in ASP Conf. Ser. 77, Astronomical Data Analysis Software
    and Systems IV, ed. R. A. Shaw, H. E. Payne, & J. J. E. Hayes (San
    Francisco, CA: ASP), 398

Torres, G. 2010, AJ, 140, 1158
Torres, G., Andersen, J., & Giménez, A. 2010, A&ARv, 18, 67
Williams, M. E. K., Steinmetz, M., Sharma, S., et al. 2011, ApJ, 728, 102
Wilson, R. E. 1979, ApJ, 234, 1054
Wilson, R. E., & Devinney, E. J. 1971, ApJ, 166, 605
Wylie-de Boer, E., Freeman, K., Williams, M., et al. 2012, ApJ, 755, 35
Zucker, S., & Mazeh, T. 1994, ApJ, 420, 806